Heliyon 9 (2023) e18047

Contents lists available at ScienceDirect

Heliyon

journal homepage: www.cell.com/heliyon

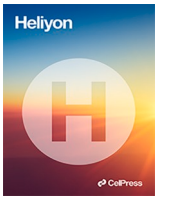

Determination of critical-sized defect of mandible in a rabbit model: Micro-computed tomography, and histological evaluation

Yue Wang [1], Xiaoyan Zhang [1], Shuang Mei, Yunlong Li, Anas Ameer Khan, Shuai Guan, Xiangjun Li [*]

Department of Oral and Maxillofacial Surgery, School and Hospital of Stomatology, Hebei Medical University & Hebei Key Laboratory of Stomatology & Hebei Clinical Research Center for Oral Diseases, Shijiazhuang, 050017, PR China

ARTICLE INFO

Keywords:
Rabbit
Laboratory animal
Mandibular defect
Bone loss
Critical-sized defect

ABSTRACT

Objective: To evaluate a rabbit model of mandibular box-shaped defects created through an intraoral approach and determine the minimum size defect that would not spontaneously heal during the rabbit's natural life (or critical-sized defect, CSD).

Methods: Forty-five 6-month-old rabbits were randomly divided into five defect size groups (nine each). Mandibular box-shaped defects of different sizes (4, 5, 6, 8, and 10 mm) were created in each hemimandible, with the same width and depth (3 and 2 mm, respectively). Four, 8, and 12 weeks post-surgery, three animals per group were euthanized. New bone formation was assessed using micro-computed tomography (MCT) and histomorphometric analyses.

Results: Box-shaped defects were successfully created in the buccal region between the incisor area and the anterior part of the mental foramen in rabbit mandibles. Twelve weeks post-surgery, MCT analysis showed that the defects in the 4, 5, and 6 mm groups were filled with new bone, while those in the 8 and 10 mm groups remained underfilled. Quantitative analysis revealed that the bone mass recovery percentage in the 8 and 10 mm groups was significantly lower than that in the other groups ($p < 0.05$). There was no significant difference in the bone mass recovery percentage between the 8 and 10 mm groups ($p > 0.05$). Histomorphometric analysis indicated that the area of new bone formation in the 8 and 10 mm groups was significantly lower than that in the remaining groups ($p < 0.05$). There was no significant difference in the new bone area between the 8 and 10 mm groups ($p > 0.05$).

Conclusions: The dimensions of box-shaped CSD created in the rabbit mandible through an intraoral approach were 8 mm × 3 mm × 2 mm. This model may provide a clinically relevant base for future tissue engineering efforts in the mandible.

1. Introduction

The mandible plays an important role in maintaining facial shape and masticatory function [1]. The aetiology of a critical-sized defect (CSD) in the mandible includes accidental trauma, infection, and tumour resection [2]. Mandibular defect can not only lead to structural damage to the mandible, resulting in noticeable bone dysfunction and deformity [3], but also significantly affect patient

* Corresponding author.
E-mail address: lixiangjun@hebmu.edu.cn (X. Li).
[1] These authors contributed equally to this paper.

https://doi.org/10.1016/j.heliyon.2023.e18047
Received 21 March 2023; Received in revised form 29 June 2023; Accepted 5 July 2023
Available online 17 July 2023

quality of life [4]. Large defects can approach or exceed the critical size, which is classically defined as the smallest size of a defect that fails to heal spontaneously without intervention over the lifetime of an animal or over the duration of the experiment [3]. In humans, a CSD will neither heal spontaneously, nor will it regenerate more than 10% of the lost bone during the patient's lifetime. Today, reconstruction of a critical-sized osseous defect is still a challenging procedure in maxillofacial surgery [2].

Animal models are often considered appropriate analogues to clinical conditions [5]. These models provide useful scientific information on the most efficient and effective ways to treat different clinical conditions [6]. Appropriate animal models offer an experimental basis for jaw tissue engineering endeavours. CSD models are the gold standard for assessing bone regeneration in preclinical studies [6]. Many factors contribute to the choice of an animal experimental model for testing bone regeneration strategies [7]. For mandibular bone regeneration, animal models are generally divided into small (including mice [8], rats [9–11], and rabbits [12–15]) and large (including dogs [16–21], goats [22,23], pigs [24,25], and monkeys [26]) animal models. Animal models usually differ in their mandibular CSDs. For example, as confirmed by several studies, the mandibular defect size is 4–5 mm in the rat model [27,28] and 15 mm without the periosteum and 50 mm with the periosteum in the canine model [29]. At present, there is no accurate experimental evidence for determining the size of a CSD to be used in New Zealand white rabbits to create jaw defect animal models. It is necessary to explore the optimal size of a CSD to provide a benchmark for future tissue engineering research.

Some studies have shown that a mandibular defect in the rabbit model is generally located in the mandibular ramus or angle [30]. However, from an anatomical point of view, the mental foramen area shows a certain degree of modelling superiority because of its rich bone marrow content, adequate bone volume, and ideal thickness [30]. Moreover, most previous experiments adopted extra-oral approaches to create a bone defect. While intraoral approaches have been proposed to be closer to the clinical reality, to date, they have rarely been implemented in animal models. In the present study, an intraoral approach was used to simulate the surgical environment of cystic lesions in the jaw and establish an animal model for different defect sizes in rabbits. The defect site was located in the buccal region between the incisor area and the anterior part of the mental foramen in the rabbit mandible.

Since the size of a CSD in the rabbit mandible has not been determined, we propose a hypothesis that if the width and depth of a rabbit box-shape defect in the mandible are determined, the length of the CSD will be between 4 and 10 mm. This study aimed to establish an animal model for a mandibular defect by using an intraoral approach and to explore the size of a CSD in the rabbit jaw to provide a clinically relevant testing ground for further mandibular tissue engineering efforts.

2. Materials and methods

2.1. Study design, animals, and experimental groups

The G* Power 3.1.9.2 software was used to statistically compute the sample size for this animal study. The input parameters were an α error probability of 0.05, an effect size f of 0.40, a power of 0.85, and 5° of freedom, as the predictor variables included 3 examination time points and 5 groups. The estimated sample size was 90 (18 rabbits/group). Mandibular surgical defects were created bilaterally (9 rabbits/group); thus, the sample size was 45 rabbits.

Forty-five healthy 6-month-old adult New Zealand white rabbits (general grade, male and female, weight 2.2–2.5 kg [average 2.4 kg]) provided by the experimental animal centre of Hebei Medical University were used for the study. The experimental animals were housed in suitably sized cages maintained at a temperature of 22 ± 2 °C and in a 12-h light/dark cycle. The animals were transferred to the laboratory environment at least 1 week before surgery to facilitate their adaptation to the new environment, check their general health status, and ensure an optimal, infection-free environment. The animals were fed with standard laboratory food and water *at libitum*. Each rabbit was housed in a separate cage to ensure comfortable access to water and food, an adequate range of motion, and a stress-free environment. Rabbits were randomly divided into five box-shaped defect groups. Box-shaped defects of 4, 5, 6, 8, and 10 mm in length, 3 mm in width, and 2 mm in depth were created in the buccal region between the incisor area and the anterior part of the mental foramen in the rabbit mandibles. Each group included nine rabbits. The study was approved by the Local Ethics Committee for Animal Experiments of Hebei Medical University (No. 2021016).

2.2. Surgical procedure

Surgically, a total of 90 cortical defects were created bilaterally in the mandibles of the rabbits. The rabbits were intravenously anesthetized using 2% pentobarbital sodium (30 mg/kg). Under general anaesthesia, the surgical site was scrubbed with a surgical

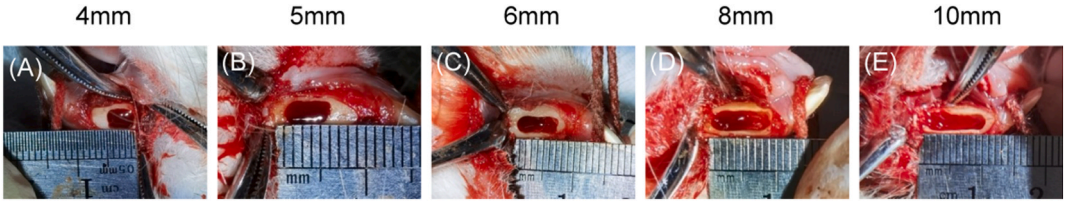

Fig. 1. Intraoperative photographs of jaw defects of different sizes. (A) The defect volume is 4 mm × 3 mm × 2 mm. (B) The defect volume is 5 mm × 3 mm × 2 mm. (C) The defect volume is 6 mm × 3 mm × 2 mm. (D) The defect volume is 8 mm × 3 mm × 2 mm. (E) The defect volume is 10 mm × 3 mm × 2 mm.

antiseptic. A 20-mm incision was made along the vestibular sulcus of the bilateral mandible of each rabbit, followed by soft tissue dissection to expose the buccal cortical bone of the anterior mandible body. The mandibular neurovascular bundle was carefully dissected and preserved. Five box-shaped osseous defects, each 3 mm in width, 2 mm in depth, and 4, 5, 6, 8, or 10 mm in length were created in the buccal region between the incisor area and the anterior part of the mental foramen in rabbit mandibles using a high-speed dental grinder and surgical drills (Fig. 1A–E). Subsequently, the surgical area was flushed with 0.9% saline solution three times to clean debris and closed in multiple layers with 4–0 sutures. The mucoperiosteal flap around the socket was sutured tightly to prevent postoperative infection. Penicillin (400,000 U/kg) was intramuscularly injected into the rabbits for 3 days post-operation. After 4, 8, and 12 weeks, three rabbits from each group were randomly euthanized by air injection into the marginal ear vein and the bone defects were evaluated using micro-computed tomography (MCT) scanning and histopathological examinations.

2.3. Radiological evaluation

Immediately after surgery, a live MCT (PerkinElmer Quantum GX micro C, PerkinElmer, USA) scan was performed to observe and measure the size and anatomical position of the defect. To compare the bone reconstruction, samples were analysed using PerkinElmer Quantum GX (Micro-CT, PerkinElmer, USA) with the following parameters: voltage, 90 kV; current, 88 μA; field of view, 36 mm; and resolution, 72 μm/pixel. Caliper Micro-CT Analysis Tools (Caliper, USA) in the analyze software were used for processing and visualization of 3D images. The region of interest was defined as a regular cuboid with 1 mm length, 2 mm width, and 1 mm height. The bone volume to total volume ratio (BV/TV) of the bone tissue in the rabbit jaw bone defect was calculated, expressed as the percentage of new bone formation, and analysed statistically.

2.4. Histological analysis

Following MCT examination, the mandibles were removed, fixed in buffered formalin for 4 h, decalcified in ethylenediaminetetraacetic acid solution, and embedded in paraffin. Serial sections were cut with a 4-μm thickness. Specimen sections were processed for routine haematoxylin and eosin (HE) staining, Masson's trichrome staining (for revealing collagen fibres and newly formed bone), and immunohistochemical staining. For immunohistochemical analysis, the deparaffinized sections were washed three times in phosphate buffer saline (PBS), and endogenous peroxidase was inactivated by incubation with 3% H2O2. Nonspecific binding sites were blocked using normal goat serum (Sigma-Aldrich, USA) for 30 min, after which the tissue sections were incubated with rabbit anti-bone morphogenetic protein 2 (BMP2) polyclonal antibody (1:100, bs-1012 R, Bioss, Beijing), anti-collagen type I (Col I) polyclonal antibody (1:100, bs-10423 R, Bioss, Beijing), anti-CD31 polyclonal antibody (1:100, bs-0195 R, Bioss, Beijing), overnight at 4 °C. After rinsing in PBS three times, the tissue sections were incubated with biotinylated secondary antibody (1:500, Z0420, DAKO, Glostrup, Denmark) at room temperature for 1 h. Peroxidase activity was visualized using 0.05% diaminobenzidine and 0.03% H2O2 in PBS. Subsequently, the tissue sections were counter-stained with haematoxylin for 2 min. At least 10 fields of vision under × 200 magnification were captured under bright-field view, and images were subsequently analysed and quantified using ImageJ software, version 1.47 (National Institutes of Health, Bethesda, MA, USA).

2.5. Histomorphometric analysis

Slides stained with HE and Masson's trichrome were analysed using an Olympus microscope. Digital images were captured by using a ToupView digital camera with an objective lens using a magnification of × 10. Five images with 300-dpi resolution from each group at each time point were digitally analysed with Fiji Image processing software, version 1.47 (National Institutes of Health, Bethesda, MA, USA). In HE staining, the percentage (%) of new bone formation was presented as the ratio of new bone area to the total defect area (NA/TA). In Masson's trichome staining, blue colour labels relatively freshly formed bone whereas red colour labels osteoid. The percentage (%) of osteoid formation was presented as the ratio of osteoid area to the total defect area (OA/TA). Positive antigen immunohistochemical staining in all sections appeared as brown staining. The average optical density value was measured to determine the levels of BMP2, Collagen type I (Col I), and CD31 expression in the bone defect area by using ImageJ software, version 1.47 (National Institutes of Health, Bethesda, MA, USA).

2.6. Data analyses

All data were expressed as the mean ± standard deviation. Statistical analysis was performed using single factor analysis of variance with SPSS version 22.0 software (SPSS, Inc., Chicago, IL, USA). A p value < 0.05 was considered statistically significant.

3. Results

3.1. Clinical findings

All surgical interventions were successfully performed without any intraoperative complications (Fig. 1A–E). All animals successfully completed the course of the study without signs of infection, debilitation, or mandibular loss of function.

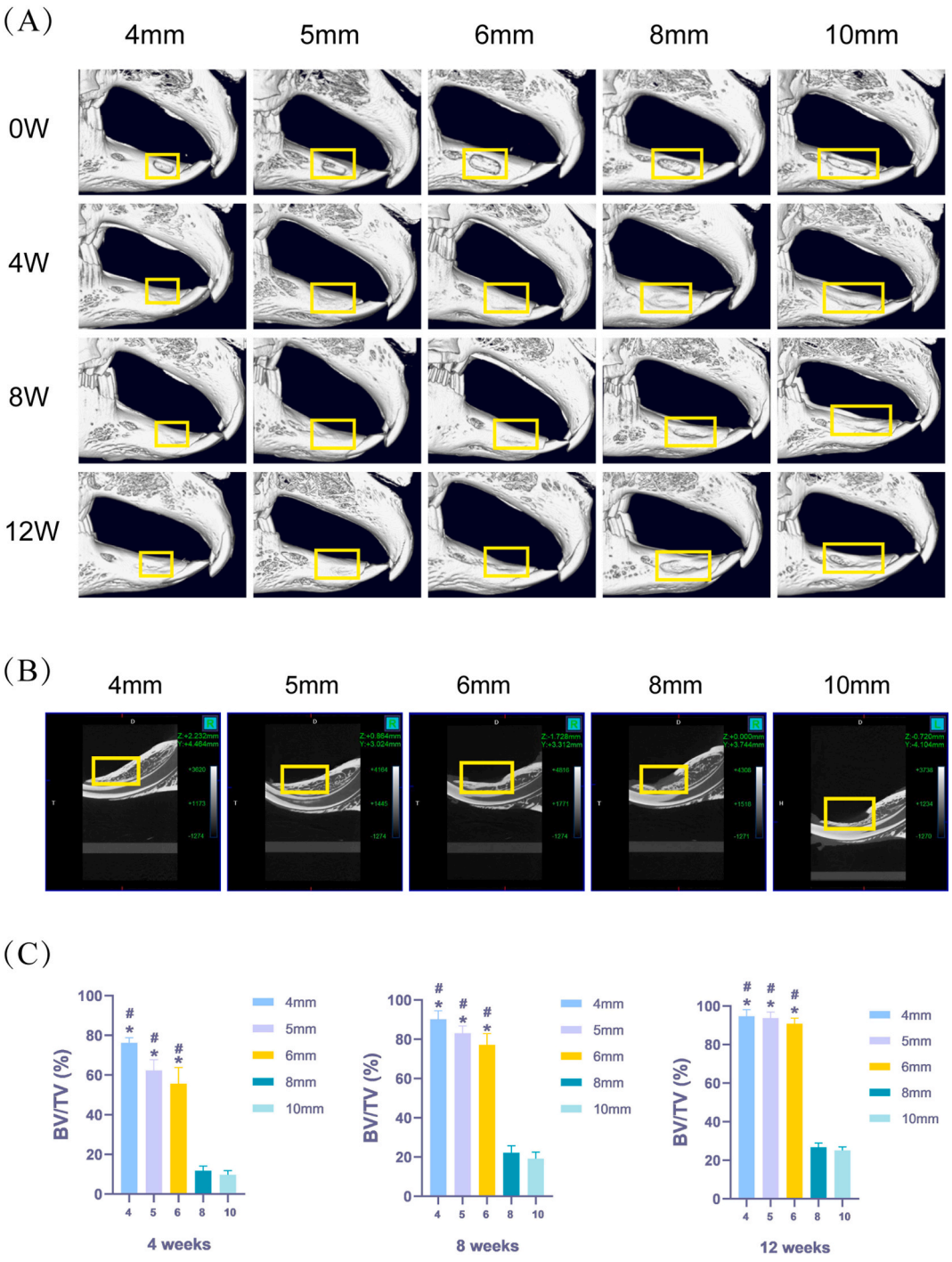

Fig. 2. Micro-computed tomography (MCT) images of jaw defects at different healing stages. (A) MCT was performed at 0 weeks, 4 weeks, 8 weeks, and 12 weeks after operation (yellow box represents the mandibular defect area). (B) Sagittal view of the jaw defect scanned by MCT at 12 weeks after operation (yellow box represents the mandibular defect area). (C) Bone volume/total volume (BV/TV) (n = 6, mean ± standard deviation) at different cycles.

*compared with the 8 mm group. The difference was statistically significant ($p < 0.05$). #compared with the 10 mm group. The difference was statistically significant ($p < 0.05$).

3.2. MCT examination

Representative 3D reconstructions of the MCT images for various groups are shown in Fig. 2A. At 4 and 8 weeks after surgery, the defect surface had healed well and new bone tissue almost completely filled the defect in the 4 and 5 mm groups. Most of the defect was filled with new bone in the 6 mm group. Only a small amount of new bone had formed and an obvious depression was observed in the 8 and 10 mm groups. At 12 weeks after surgery, the defects in the 4, 5, and 6 mm groups were filled with new bone, while the defects in the 8 and 10 mm groups were still underfilled with new bone (Fig. 2B).

One-way analysis of variance results for BV/TV revealed that the amounts of new bone formation in the 4, 5, and 6 mm groups were significantly higher than those in the 8 and 10 mm groups at different time points (Fig. 2C). At 4, 8, and 12 weeks, the 8 mm (11.75 ± 2.15%, 22.22 ± 3.29%, and 26.78 ± 2.00%, respectively) and 10 mm (9.76 ± 2.01%, 19.17 ± 3.33%, and 25.12 ± 1.86%, respectively) groups exhibited low mean values for new bone formation compared to all other groups. The BV/TV of the 8 and 10 mm groups was significantly lower ($p < 0.05$) than the 4, 5, and 6 mm groups. There was no significant difference in BV/TV between the 8 and 10 mm groups ($p > 0.05$).

3.3. HE staining results

In the 4, 5, and 6 mm groups, the bone defects showed the presence of small islands of non-lamellar bone surrounded by dense fibrous connective tissue at 4 weeks postoperatively. At 8 weeks postoperatively, the original defect was filled with a large amount of new bony tissue, with small areas of granulation tissue. At 12 weeks postoperatively, the defects were almost completely closed with high-quality lamellar, new bony tissue (Fig. 3A).

At 4 weeks postoperatively, the empty bone defects showed loose connective tissue consisting of a meshwork of fine, irregularly arranged collagen fibres in the 8 and 10 mm groups. At 8 weeks postoperatively, the largest part of the defects remained free of bone,

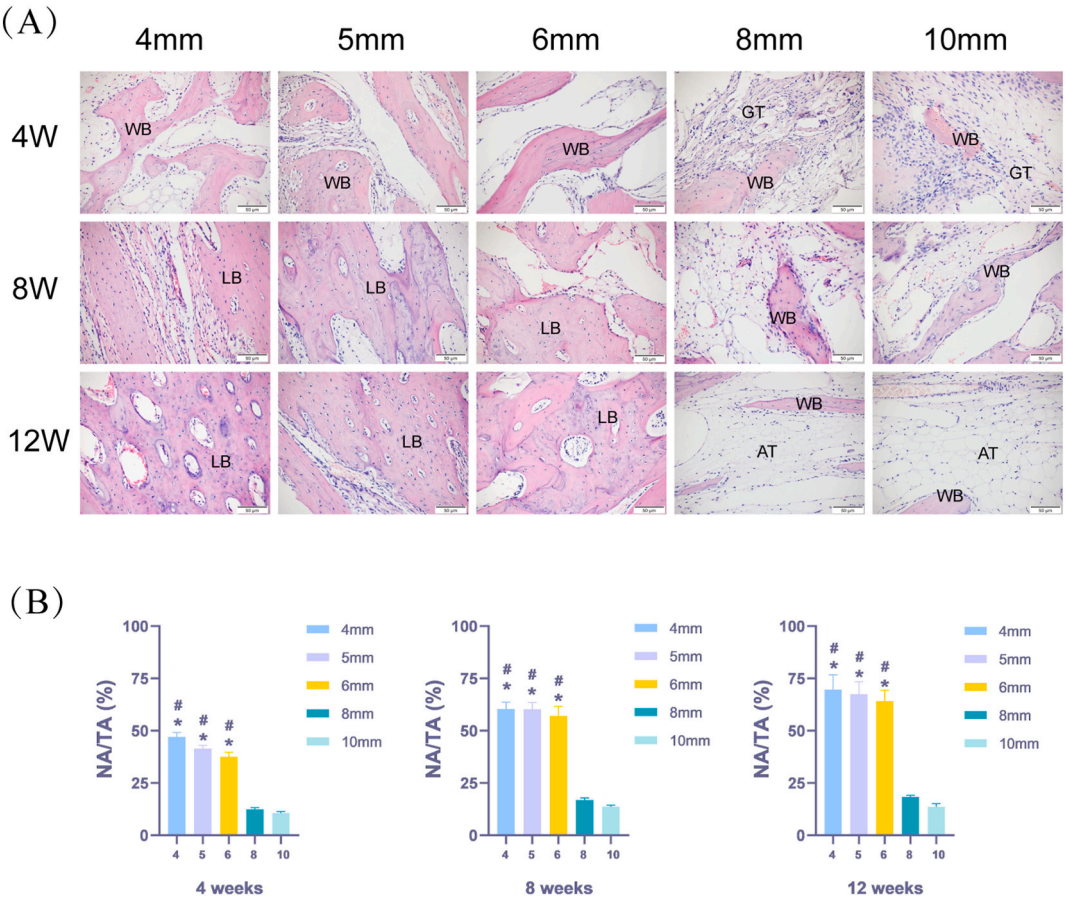

Fig. 3. Haematoxylin-eosin staining results. (A) Histological observation of jaw defects at different healing stages (HE staining × 100) (GT: granulation tissue, WB: woven bone, LB: lamellar bone, AT: adipose tissue). (B) New bone area/total defect area (NA/TA) (n = 6, mean ± standard deviation) at different cycles.

*compared with the 8 mm group. The difference was statistically significant ($p < 0.05$). #compared with the 10 mm group. The difference was statistically significant ($p < 0.05$).

with a sparse amount of thin osteoid bone trabeculae separated by a substantial amount of amorphous ground substance. At 12 weeks postoperatively, the bone defect area remained predominantly free of bone, and was filled only with connective tissue that contained few cells and many collagen fibres with a minute amount of newly formed bone trabeculae (Fig. 3A).

Histomorphometric measurements using HE staining images at different time points revealed significant differences in bone formation. The percentages of new bone formation in the 8 and 10 mm groups were significantly lower than those in the 4, 5, and 6 mm groups at different time points. At 4, 8, and 12 weeks, the 8 mm (12.411 ± 0.717%, 16.905 ± 0.851%, and 18.261 ± 0.817%, respectively) and 10 mm (10.659 ± 0.692%, 13.548 ± 1.033%, and 13.596 ± 1.364%, respectively) groups exhibited low mean values of percentage of new bone formation, compared to all other groups. The percentages of new bone formation in the 8 and 10 mm groups were significantly lower ($p < 0.05$) than in the 4, 5, and 6 mm groups. There was no significant difference in the percentage of new bone formation between the 8 and 10 mm groups ($p > 0.05$) (Fig. 3B).

3.4. Masson's trichrome staining results

In the 4, 5, and 6 mm groups, the empty bone defects showed a considerable number of bony islands enclosed by dense connective tissue of blue colour at 4 weeks postoperatively. At 8 weeks postoperatively, the amount of new bone formation was significantly increased. Immature lamellar bone tissue and red-stained, newly formed osteoid were observed in the bone defect area. The development of high-quality lamellar, mature bone was clearly observed at 12 weeks postoperatively. The defects were ultimately filled with bone and revealed an intricate integration of newly formed osteoid tissue with the old mature, lamellar bone.

In the 8 and 10 mm groups, the defects were observed as scattered bony islands at 4 weeks postoperatively. At 8 weeks postoperatively, a small number of thin strips of bone tissue could be seen in the defects with wide gaps. At 12 weeks postoperatively, the

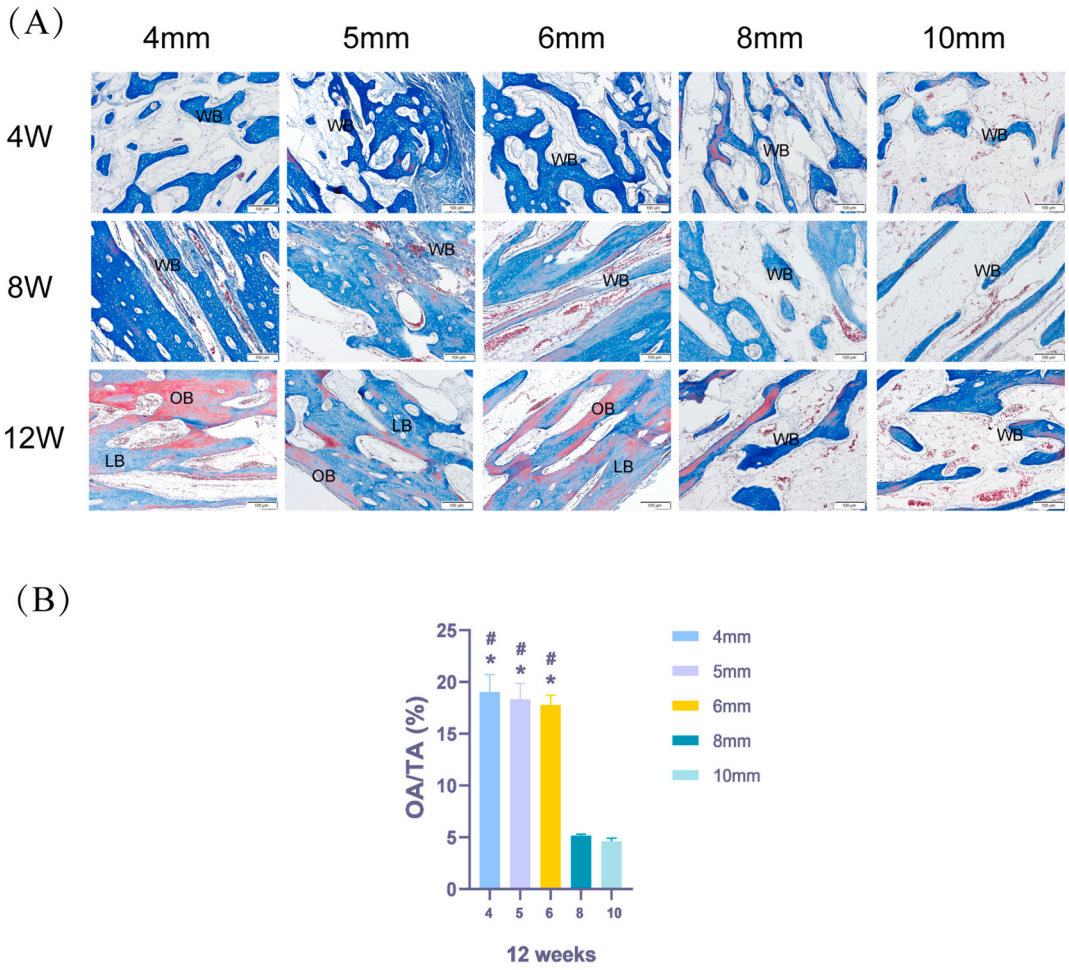

Fig. 4. Masson's trichrome staining results. (A) Histological observation of jaw defects at different healing stages (Masson's stain × 100) (OB: osteoid, WB: woven bone, LB: lamellar bone). (B) Osteoid area/total defect area (OA/TA) (n = 6, mean ± standard deviation) at different cycles. *compared with the 8 mm group. The difference was statistically significant ($p < 0.05$). #compared with the 10 mm group. The difference was statistically significant ($p < 0.05$).

bone defects were filled with abundant loose irregular connective tissue with a very small amount of blue-stained trabecular tissue across the entire defect (Fig. 4A).

Osteoid formation was generally observed at 12 weeks. At 12 weeks after surgery, the osteoid ratios in the 8 mm (5.160 ± 0.142%) and 10 mm (4.617 ± 0.255%) groups were significantly lower than those in the 4 mm (19.026 ± 1.543%), 5 mm (18.320 ± 1.404%), and 6 mm (17.778 ± 0.855%) groups. The osteoid ratios in the 8 and 10 mm groups were significantly lower ($p < 0.05$) than in the 4, 5, and 6 mm groups. There was no significant difference in the osteoid ratio between the 8 and 10 mm groups ($p > 0.05$) (Fig. 4B).

3.5. Immunohistochemical results

3.5.1. Expression of BMP2

At 4, 8, and 12 weeks after surgery, the expression of BMP2 showed no statistical differences among any group ($p > 0.05$, Fig. 5A and B).

3.5.2. Expression of col I

The expression levels of Col I in the 4, 5, and 6 mm groups were significantly higher than those in the 8 and 10 mm groups at 4 weeks. In contrast, the expression levels of Col I in the 4, 5, and 6 mm groups were significantly lower than those in the 8 and 10 mm groups at 8 weeks (Fig. 6A). Col I expression was consistent in all the groups at 12 weeks (Fig. 6A). At 4 weeks postoperatively, the expression levels of Col I in the 8 and 10 mm groups were significantly lower ($p < 0.05$) than in the 4, 5, and 6 mm groups. There was no significant difference in the expression of Col I between the 8 and 10 mm groups ($p > 0.05$). At 8 weeks postoperatively, the expression levels of Col I in the 8 and 10 mm groups were significantly higher ($p < 0.05$) than in the 4, 5, and 6 mm groups. There was no significant difference in the expression of Col I between the 8 and 10 mm groups ($p > 0.05$). At 12 weeks after surgery, the expression of Col I showed no statistical differences among any group ($p > 0.05$) (Fig. 6B).

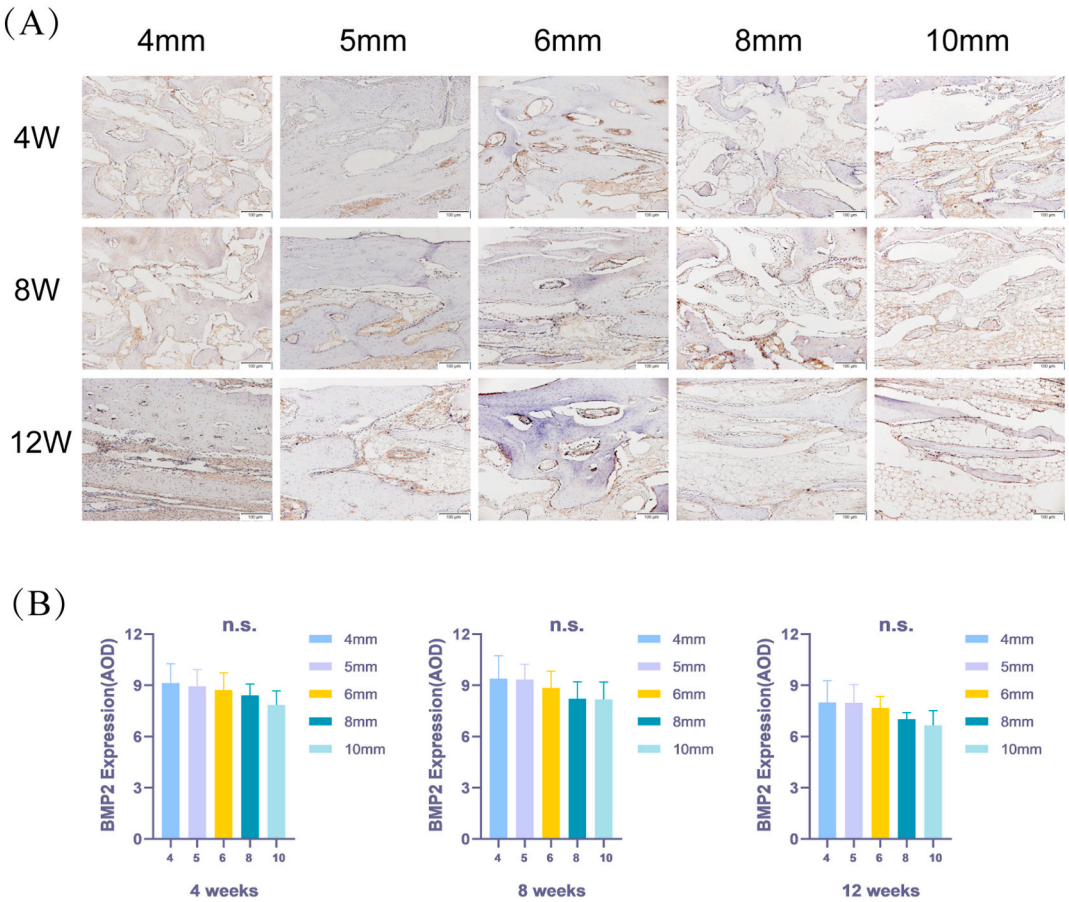

Fig. 5. Bone morphogenic protein 2 (BMP2) immunostaining results. (A) Immunohistochemical observation of jaw defects at different healing stages (BMP2 immunostaining × 100). (B) BMP2 expression (n = 6, mean ± standard deviation) was consistent in the 4 mm, 5 mm, 6 mm, 8 mm, and 10 mm groups at different cycles. There was no significant difference among groups ($p > 0.05$). n. s., not significant.

3.5.3. Expression of CD31

At 4, 8, and 12 weeks after surgery, the expression of CD31 showed no statistical differences among any group ($p > 0.05$, Fig. 7A and B).

4. Discussion

This study focused on how to replicate mandibular defects in an appropriate animal model. The advantages of rat models are lower cost and convenience, which includes ease of housing and care. However, the limitations in body size and bone mass make them unsuitable for studying the osteogenic ability of materials, and the differences in relative osteogenic speed make them unsuitable for direct extrapolation in the patient populations [31]. As for large animals such as dogs, goats, and pigs, their use is limited by their high prices and farming conditions, and their special status as human companions raises more ethical questions. Meanwhile, rabbits rank first among all animals used for musculoskeletal research [3]. The rabbit mandible is physically larger than the rat mandible, making surgical procedures less technically demanding [31]. Thus, a suitable mandibular defect with enough volume to support a potential synthetic scaffold can be created in rabbits. Importantly, rabbits appear to exhibit basic multicellular unit remodelling that is naturally occurring (similar to that in humans). Moreover, rabbits have a cortical bone modulus and strength that are more similar than other animals to humans [31]. All these factors make rabbits more suitable for bone regeneration research studies. Considering both practicality and costs, we chose the New Zealand white rabbit as the best animal to establish a jaw defect model through an intraoral approach.

The regenerative cell populations and environment present in the mandible and oral cavity are unique and cannot be replicated in other anatomical parts [7]. An intraoral approach better simulates the surgical and postoperative oral environment of jaw cysts and tumours. Another reason that rabbits are often selected as animal models for jaw defects is that their premolars and/or molars have

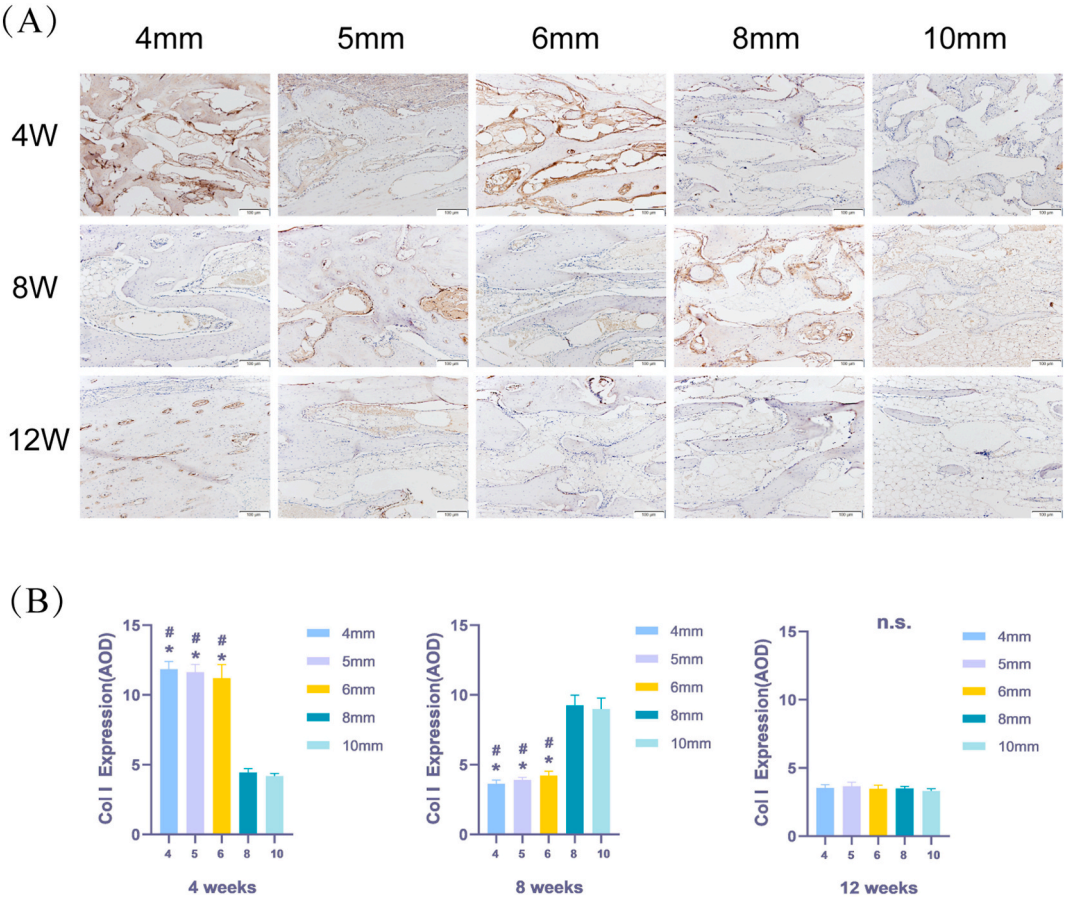

Fig. 6. Collagen type I (Col I) immunostaining results. (A) Immunohistochemical observation of jaw defects at different healing stages (Col I immunostaining × 100). (B) Col I expression (n = 6, mean ± standard deviation) at different cycles.
*compared with the 8 mm group. The difference was statistically significant ($p < 0.05$).
#compared with the 10 mm group. The difference was statistically significant ($p < 0.05$).
Col I expression (n = 6, mean ± standard deviation) was consistent in the 4 mm, 5 mm, 6 mm, 8 mm, and 10 mm groups at 12 weeks. There was no significant difference among groups ($p > 0.05$). n. s., not significant.

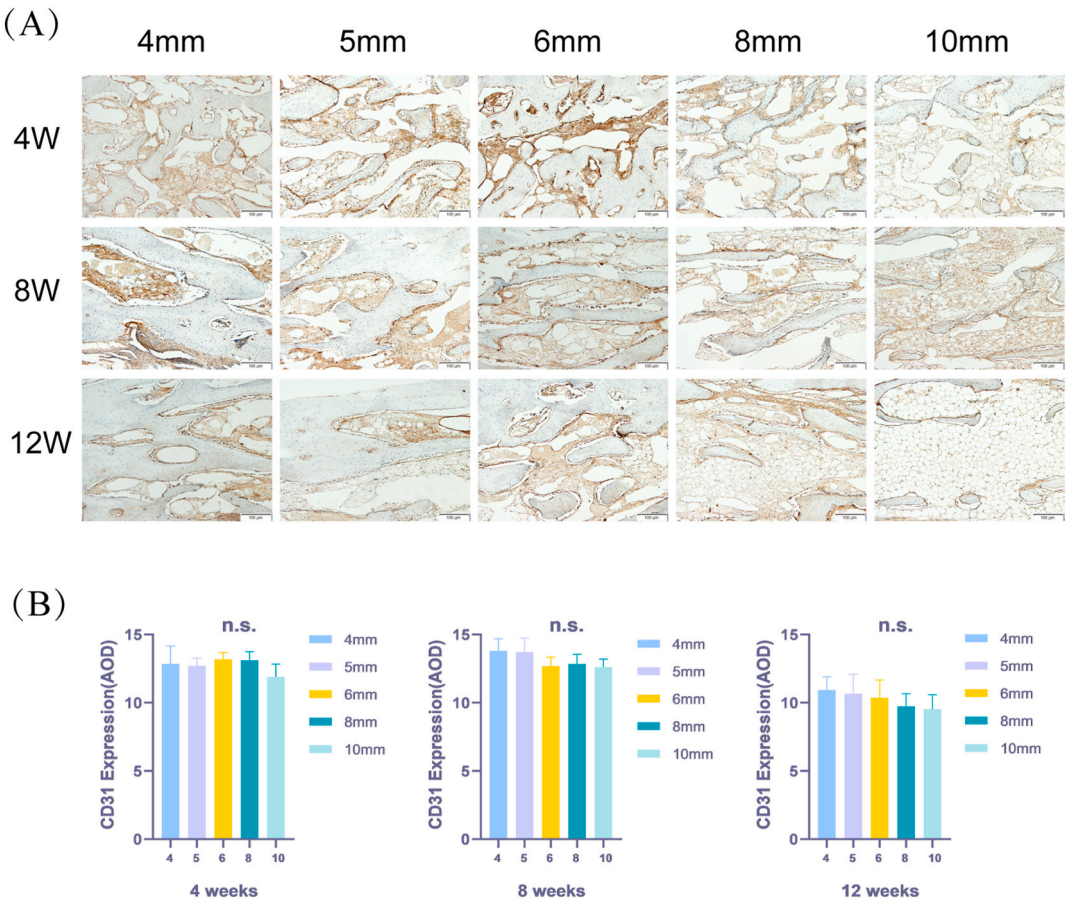

Fig. 7. CD31 immunostaining results. (A) Immunohistochemical observation of jaw defects at different healing stages (CD31 immunostaining × 100). (B) CD31 expression (n = 6, mean ± standard deviation) was consistent in the 4 mm, 5 mm, 6 mm, 8 mm, and 10 mm groups at different cycles. There was no significant difference among groups ($p > 0.05$). n. s., not significant.

adequately-sized alveolar bone tissue (17-mm long, 16-mm high, and 6-mm thick) [7]. Therefore, in this study, an intraoral approach was selected to simulate the oral environment of cyst curettage. The mandibular foramina region with teeth was selected as the study site to explore CSDs in the rabbit jaw defect animal model.

Different animal models present different CSDs in the mandible. The mandibular defect size of 4–5 mm in the rat model [27,28] and of 15 mm without periosteum and 50 mm with periosteum in the canine model was confirmed by several studies [27,28]. Zongyang et al. confirmed that 5-cm^3 defects in the mandibular angle region without buccal periosteum in 4-month-old pigs would be a reasonable CSD model relevant to mandibular defects in adolescent humans [32]. Few studies have used sheep or primates as animal models of bone defects, and no studies on CSDs in sheep or primates have been reported so far. In the case of notch-type defects in the rabbit model, multiple studies have evaluated defects of various sizes at different locations in the mandible with little consistency, leading to great difficulty in comparing results across studies [33]. At present, there is no accurate experimental evidence for the size of CSDs to be used in New Zealand white rabbits to establish jaw defect animal models. A defect diameter greater than 5 mm in the rabbit mandible has been reported to be a critical size that prevents spontaneous healing [34]. Other scholars believe that lengths of 10 mm can be used in rabbits for bone defect models [35]. Therefore, it is necessary to explore the optimal size of a CSD to provide a benchmark for future tissue engineering research.

Monir et al. suggested that the defect type also significantly influences the resorption rate of bone regeneration materials [2]. This study intended to produce a defect with sufficient volume to store a scaffold or material, which requires a certain width and depth. Therefore, a box-shaped mandibular bone defect was considered suitable in terms of shape and size. In pre-experiments, the rabbit mandible was dissected and the region suitable for maximum defect length was identified in the anterior part of the mandible. The width of the box-shaped defect was set at 3 mm, because the maximum width for producing a defect in this area is approximately 3 mm. The maximum length from this area to the mental foramen was approximately 10 mm to avoid injury to the mental nerve and mandibular fracture. A high-speed dental grinder was used to create the defects. The diameter and length of the working end of the ball drill were both 2 mm, which guaranteed accuracy when making a bone defect with a width of 3 mm, depth of 2 mm, and length 4–10 mm. On the other hand, avoiding interference with ischemia stemming from the bone defect areas is important in establishing mandibular bone defect models. The presence of the periosteum and neurovascular bundle has been proven to play an important role

in the repair of CSDs [29,31]. In the present study, the periosteum and the mental nerve were carefully preserved during defect creation, which prevented the loss of local blood circulation from affecting the process of osteogenesis in the CSD region.

MCT is a nondestructive method that can be employed for both visualization and structural evaluation of newly formed bone [1]. First introduced by Feldkamp et al. in the late 1980s [36], MCT has now become the 'gold standard' for evaluating bone morphology and micro-architecture in small, living animal models. Assessment of bone morphology by MCT scanning is nondestructive; thus, samples can be used subsequently for other assays, such as histology or mechanical testing [37]. Collecting MCT data in rats is straightforward when using a high-resolution small mammal CT scanner. However, it was more challenging with rabbits, as the same MCT scanner could not be used given that the rabbits were too large for the imaging chamber. Similar to other studies [2], the animals were sacrificed at 4, 8, and 12 weeks postoperatively. Under both projection and 3D reconstruction, we found that bone defects above 8 mm in diameter were not completely repaired under natural healing conditions. In contrast, the bone defects in the 4 mm, 5 mm, and 6 mm groups repaired naturally, suggesting that size of a box-shaped CSD in the rabbit mandibular bone defect model was 8 mm $\times$ 3 mm $\times$ 2 mm.

To confirm the observations of MCT histologically, HE and Masson's trichrome staining was performed for histomorphological analysis. The results were consistent with those obtained through MCT. At 12 weeks postoperatively, as shown by histological staining, a small amount of new trabecular bone and more adipose tissue appeared in the bone defect area when the defect diameter reached above 8 mm. As shown by histomorphological analysis, the absolute amount of new bone was significantly reduced, which was in accordance with the decrease in BV/TV (relative amount) observed by MCT analysis. An increase in defect volume seemed to affect the formation of new bone.

To start exploring the reasons for the reduction in new bone formation beyond the CSD value, we investigated the expressions at different time points of BMP2, Col I, and CD31 in the bone defects. As an interesting result, the expression of Col I, the specific protein for matrix deposition in the skeletal tissue at the later stages of osteogenesis [30], was higher in the 4 mm, 5 mm, and 6 mm groups at 4 weeks. On the contrary, Col I showed higher expression at 8 weeks in the 8 mm and 10 mm groups. At 12 weeks, the expression of Col I showed no significant differences among the five groups. The results suggested that the upregulation of Col I may be helpful at the early stages of osteogenesis, especially within 4 weeks in the rabbit model. However, we failed to find statistical differences in the expressions of BMP2 and CD31. BMP2 is a marker protein for the initial stage of osteogenesis. The role of BMP is well-established in bone tissue engineering applications due to its ability to recruit mesenchymal cell differentiation. At the same time, angiogenesis is one of the most important factors for bone formation. CD31 is a specific marker of endothelial cells that is highly expressed during bone formation [38]. The absence of differences in the expressions of BMP2 and CD31 during the osteogenesis process among the five groups indicated that the characteristics of these bones were similar. Moreover, the osteogenic differentiation process lasted from the early to the late healing stages. These findings are consistent with the results reported in previous studies [39]. The mechanism underlying the failure of CSD to heal without intervention over the animal's lifetime is still unknown. According to the present results, it is concluded that the high expression of Col I in the early stage of bone defect healing may positively impact the spontaneous repair of CSD. The underlying functional mechanism needs to be further studied. The noticeable bone formation in small bone defects at 4 weeks showed the necessity to observe bones at earlier stages, such as 2 weeks after surgery.

5. Conclusions

An intraoral approach was used to establish box-shaped mandibular bone defects in rabbits. The critical bone defect volume in the rabbit mandibular defect model was found to be 8 mm $\times$ 3 mm $\times$ 2 mm. High expression of Col I in the early stage of bone defect healing may positively impact spontaneous CSD repair. The model may provide a clinically relevant testing ground for future tissue engineering efforts in the mandible.

Authors' contributions

Yue Wang: Performed the experiments; Analysed and interpreted the data; Wrote the paper.
Xiaoyan Zhang: Performed the experiments; Contributed reagents, materials, analysis tools or data; Wrote the paper.
Shuang Mei and Yunlong Li: Performed the experiments; Contributed reagents, materials, analysis tools or data.
Anas Ameer Khan and Shuai Guan: Analysed and interpreted the data; Contributed reagents, materials, analysis tools or data.
Xiangjun Li: Conceived and designed the experiments; Wrote the paper.

Data availability statement

All the data used in the present study are available from the corresponding author upon reasonable request.

Declaration of competing interest

The authors declare that they have no known competing financial interests or personal relationships that could have appeared to influence the work reported in this paper.

Acknowledgements

This study was supported by a grant-in-aid for the program of the government funding for clinical medicine excellence training of Hebei Province (no. 2020048149-2), a grant-in-aid for The Health Innovation Project of Hebei Provincial Science and Technology Plan (no. 21377719D), and a grant-in-aid for The Youth Science and Technology Projects Foundation of Health commission of Hebei Province (no. 20191082).

References

[1] C.G. Koca, M. Kösehasanoğulları, Evaluation of single-dose applied teriparatide effect on bone healing with histomorphometric and micro-ct analysis, J Cranio Maxill Surg 49 (2) (2021) 98–103, https://doi.org/10.1016/j.jcms.2020.12.004.
[2] A. Monir, T. Mukaibo, A.B.M. Abd El-Aal, T. Nodai, T. Munemasa, Y. Kondo, C. Masaki, M.A. El-Shair, K. Matsuo, R. Hosokawa, Local administration of HMGB-1 promotes bone regeneration on the critical-sized mandibular defects in rabbits, Sci Rep-Uk 11 (1) (2021), https://doi.org/10.1038/s41598-021-88195-7.
[3] A.A. Ashour, M. Zaghloul, W. Mahmoud, M.E. Helal, M.E. Grawish, Gelfoam haemostatic agent with or without autologous bone marrow-derived stem cells for the regeneration of critical-size mandibular defects in the rabbit, Int. J. Oral Maxillofac. Surg. 47 (11) (2018) 1488–1494, https://doi.org/10.1016/j.ijom.2018.04.021.
[4] Y. Cui, C. Lu, B. Chen, J. Han, Y. Zhao, Z. Xiao, S. Han, J. Pan, J. Dai, Restoration of mandibular bone defects with demineralized bone matrix combined with three-dimensional cultured bone marrow-derived mesenchymal stem cells in minipig models, J. Mater. Sci. Mater. Med. 29 (9) (2018), https://doi.org/10.1007/s10856-018-6152-3.
[5] M.A. Awadeen, F.A. Al-Belasy, L.E. Ameen, M.E. Helal, M.E. Grawish, Early therapeutic effect of platelet-rich fibrin combined with allogeneic bone marrow-derived stem cells on rats' critical-sized mandibular defects, World J. Stem Cell. 12 (1) (2020) 55–69, https://doi.org/10.4252/wjsc.v12.i1.55.
[6] C.G. Trejo-Iriarte, J. Serrano-Bello, R. Gutiérrez-Escalona, C. Mercado-Marques, N. García-Honduvilla, J. Buján-Varela, L.A. Medina, Evaluation of bone regeneration in a critical size cortical bone defect in rat mandible using microCT and histological analysis, Arch. Oral Biol. 101 (2019) 165–171, https://doi.org/10.1016/j.archoralbio.2019.01.010.
[7] S.R. Shah, S. Young, J.L. Goldman, J.A. Jansen, M.E. Wong, A.G. Mikos, A composite critical-size rabbit mandibular defect for evaluation of craniofacial tissue regeneration, Nat. Protoc. 11 (10) (2016) 1989–2009, https://doi.org/10.1038/nprot.2016.122.
[8] M.H. Mankani, S.A. Kuznetsov, R.M. Wolfe, G.W. Marshall, P.G. Robey, In vivo bone formation by human bone marrow stromal cells: reconstruction of the mouse calvarium and mandible, Stem Cell. 24 (9) (2006) 2140–2149, https://doi.org/10.1634/stemcells.2005-0567.
[9] M. Dréno, P. Bléry, J. Guicheux, P. Weiss, O. Malard, F. Espitalier, Development of a rat model of mandibular irradiation sequelae for preclinical studies of bone repair, Tissue Eng. C Methods 26 (8) (2020) 447–455, https://doi.org/10.1089/ten.tec.2020.0109.
[10] E. Özkan, M.C. Bereket, E. Şenel, M.E. Önger, Effect of electrohydraulic extracorporeal shockwave therapy on the repair of bone defects grafted with particulate allografts, J. Craniofac. Surg. 30 (4) (2019) 1298–1302, https://doi.org/10.1097/SCS.0000000000005213.
[11] F.J. Barrientos, L.M. Redondo, M. Alberca, A.M. Sánchez, J. García-Sancho, Bone regeneration with autologous adipose-derived mesenchymal stem cells: a reliable experimental model in rats, MethodsX 7 (2020), 101137, https://doi.org/10.1016/j.mex.2020.101137.
[12] S. Kotagudda Ranganath, M. Schlund, J. Delattre, J. Ferri, F. Chai, Bilateral double site (calvarial and mandibular) critical-size bone defect model in rabbits for evaluation of a craniofacial tissue engineering constructs, Materials Today Bio 14 (2022), 100267, https://doi.org/10.1016/j.mtbio.2022.100267.
[13] M. V, S. Iyer, D. Menon, S.V. Nair, M.B. Nair, Evaluation of osseointegration of staged or simultaneously placed dental implants with nanocomposite fibrous scaffolds in rabbit mandibular defect, Mater. Sci. Eng. C 104 (2019), 109864, https://doi.org/10.1016/j.msec.2019.109864.
[14] S.L. Piotrowski, L. Wilson, K.L. Maldonado, R. Tailor, L.R. Hill, J.A. Bankson, S. Lai, F.K. Kasper, S. Young, Effect of radiation on DCE-MRI pharmacokinetic parameters in a rabbit model of compromised maxillofacial wound healing: a pilot study, J. Oral Maxillofac. Surg. 78 (6) (2020) 1031–1034, https://doi.org/10.1016/j.joms.2020.02.001.
[15] Y. Bai, X. Dai, Y. Yin, J. Wang, X. Sun, W. Liang, Y. Li, X. Deng, X. Zhang, Biomimetic piezoelectric nanocomposite membranes synergistically enhance osteogenesis of deproteinized bovine bone grafts, Int. J. Nanomed. 14 (2019) 3015–3026, https://doi.org/10.2147/IJN.S197824.
[16] S.K. Anwar, H.M.A. Hamid, Immuno-histopathologic evaluation of mineralized plasmatic matrix in the management of horizontal ridge defects in a canine model (a split-mouth comparative study), Odontology 110 (3) (2022) 523–534, https://doi.org/10.1007/s10266-021-00684-3.
[17] A.H. Mesgarzadeh, I. Nasiri, S. Jarolmasjed, M. Naghibi, H. Shafaei, Evaluation of bone regeneration in mandible large defect using undifferentiated adipose stem cells loaded on gelatin carrier: an animal model case study, J. Dent. Res. Dent. Clin. Dent. Prospects 15 (1) (2021) 22–29, https://doi.org/10.34172/joddd.2021.005.
[18] J. Wu, Q. Wang, X. Fu, X. Wu, C. Gu, J. Bi, F. Xie, N. Kang, X. Liu, L. Yan, Y. Cao, R. Xiao, Influence of immunogenicity of allogeneic bone marrow mesenchymal stem cells on bone tissue engineering, Cell Transplant. 25 (2) (2016) 229–242, https://doi.org/10.3727/096368915X687967.
[19] B. Rai, K.H. Ho, Y. Lei, K. Si-Hoe, C. Jeremy Teo, K.B. Yacob, F. Chen, F. Ng, S.H. Teoh, Polycaprolactone-20% tricalcium phosphate scaffolds in combination with platelet-rich plasma for the treatment of critical-sized defects of the mandible: a pilot study, J. Oral Maxillofac. Surg. 65 (11) (2007) 2195–2205, https://doi.org/10.1016/j.joms.2006.11.026.
[20] A. Khojasteh, H. Behnia, F.S. Hosseini, M.M. Dehghan, P. Abbasnia, F.M. Abbas, The effect of PCL-TCP scaffold loaded with mesenchymal stem cells on vertical bone augmentation in dog mandible: a preliminary report, J. Biomed. Mater. Res. B Appl. Biomater. 101 (5) (2013) 848–854, https://doi.org/10.1002/jbm.b.32889.
[21] S. Lee, D. Choi, J.H. Shim, W. Nam, Efficacy of three-dimensionally printed polycaprolactone/beta tricalcium phosphate scaffold on mandibular reconstruction, Sci. Rep. 10 (1) (2020) 4979, https://doi.org/10.1038/s41598-020-61944-w.
[22] M.E.L. Nienhuijs, X.F. Walboomers, A. Briest, M.A.W. Merkx, P.J.W. Stoelinga, J.A. Jansen, Healing of bone defects in the goat mandible, using COLLOSS registered E and Delta b-tricalciumphosphate, J. Biomed. Mater. Res., Part B 92B (2) (2010) 517–524, https://doi.org/10.1002/jbm.b.31546.
[23] L. Zhou, H. Shang, M. Hu, D. Li, S. Sigare, B. Chen, Y. Liu, J. Zhao, Reconstruction of curved mandibular angle defects using a new internal transport distraction device: an experiment in goats, Br. J. Oral Maxillofac. Surg. 46 (6) (2008) 445–448, https://doi.org/10.1016/j.bjoms.2008.01.006.
[24] K. Dienel, A. Abu-Shahba, R. Kornilov, R. Bjorkstrand, B. van Bochove, J. Snall, T. Wilkman, K. Mesimaki, A. Meller, J. Linden, A. Lappalainen, J. Partanen, R. Seppanen-Kaijansinkko, J. Seppala, B. Mannerstrom, Patient-specific bioimplants and reconstruction plates for mandibular defects: production workflow and in vivo large animal model study, Macromol. Biosci. 22 (4) (2022), e2100398, https://doi.org/10.1002/mabi.202100398.
[25] B.A.J.A. van Oirschot, E.J.W. Geven, A.G. Mikos, J.J.J.P. van den Beucken, J.A. Jansen, A mini-pig mandibular defect model for evaluation of craniomaxillofacial bone regeneration, Tissue Eng. C Methods 28 (5) (2022) 193–201, https://doi.org/10.1089/ten.tec.2022.0012.
[26] Y. Xie, Y. Su, S. Min, J. Tang, B.T. Goh, L. Saigo, S. Ansari, A. Moshaverinia, C. Zhang, J. Wang, Y. Liu, A. Khojasteh, H.H. Zadeh, S. Wang, Collagen sponge functionalized with chimeric anti-BMP-2 monoclonal antibody mediates repair of critical-size mandibular continuity defects in a nonhuman primate model, BioMed Res. Int. 2017 (2017) 1–11, https://doi.org/10.1155/2017/8094152.
[27] P.A. Miguez, S.A. Tuin, A.G. Robinson, J. Belcher, P. Jongwattanapisan, K. Perley, V. de Paiva Gonçalves, A. Hanifi, N. Pleshko, E.R. Barton, Hesperidin promotes osteogenesis and modulates collagen matrix organization and mineralization in vitro and in vivo, Int. J. Mol. Sci. 22 (6) (2021) 3223, https://doi.org/10.3390/ijms22063223.
[28] W. Zhang, W. Shi, S. Wu, M. Kuss, X. Jiang, J.B. Untrauer, S.P. Reid, B. Duan, 3D printed composite scaffolds with dual small molecule delivery for mandibular bone regeneration, Biofabrication 12 (3) (2020), 35020, https://doi.org/10.1088/1758-5090/ab906e.
[29] J.Y. Huh, B.H. Choi, B.Y. Kim, S.H. Lee, S.J. Zhu, J.H. Jung, Critical size defect in the canine mandible, Oral Surg. Oral Med. Oral Pathol. Oral Radiol. Endod. 100 (3) (2005) 296–301, https://doi.org/10.1016/j.tripleo.2004.12.015.

[30] J. Guo, Z. Meng, G. Chen, D. Xie, Y. Chen, H. Wang, W. Tang, L. Liu, W. Jing, J. Long, W. Guo, W. Tian, Restoration of critical-size defects in the rabbit mandible using porous nanohydroxyapatite-polyamide scaffolds, Tissue Eng. 18 (11–12) (2012) 1239–1252, https://doi.org/10.1089/ten.tea.2011.0503.
[31] J.Z. Baskin, B.M. White, A. Vasanji, T.E. Love, S.J. Eppell, Mandible biomechanics and continuously erupting teeth: a new defect model for studying load-bearing biomaterials, Biomedicines 9 (7) (2021) 730, https://doi.org/10.3390/biomedicines9070730.
[32] Z. Sun, K.S. Kennedy, B.C. Tee, J.B. Damron, M.J. Allen, Establishing a critical-size mandibular defect model in growing pigs: characterization of spontaneous healing, J. Oral Maxillofac. Surg. 72 (9) (2014) 1852–1868, https://doi.org/10.1016/j.joms.2014.02.024.
[33] P.L. Carlisle, T. Guda, D.T. Silliman, R.G. Hale, P.R. Brown Baer, Are critical size bone notch defects possible in the rabbit mandible? J. Korean Assoc. Oral and Maxillofacial Surgeons 45 (2) (2019) 97, https://doi.org/10.5125/jkaoms.2019.45.2.97.
[34] X. Wang, H. Xing, G. Zhang, X. Wu, X. Zou, L. Feng, D. Wang, M. Li, J. Zhao, J. Du, Y. Lv, , L. E, H. Liu, Restoration of a critical mandibular bone defect using human alveolar bone-derived stem cells and porous nano-HA/collagen/PLA scaffold, Stem Cell. Int. (2016) 1–13, https://doi.org/10.1155/2016/8741641.
[35] G. Cheng, Z. Li, Q. Wan, K. Lv, D. Li, X. Xing, Z. Li, A novel animal model treated with tooth extraction to repair the full-thickness defects in the mandible of rabbits, J. Surg. Res. 194 (2) (2015) 706–716, https://doi.org/10.1016/j.jss.2014.11.010.
[36] L.A. Feldkamp, S.A. Goldstein, A.M. Parfitt, G. Jesion, M. Kleerekoper, The direct examination of three-dimensional bone architecture in vitro by computed tomography, J. Bone Miner. Res. 4 (1) (1989) 3–11, https://doi.org/10.1002/jbmr.5650040103.
[37] M.L. Bouxsein, S.K. Boyd, B.A. Christiansen, R.E. Guldberg, K.J. Jepsen, R. Müller, Guidelines for assessment of bone microstructure in rodents using micro-computed tomography, J. Bone Miner. Res. 25 (7) (2010) 1468–1486, https://doi.org/10.1002/jbmr.141.
[38] J. Kim, I.S. Kim, T.H. Cho, K.B. Lee, S.J. Hwang, G. Tae, I. Noh, S.H. Lee, Y. Park, K. Sun, Bone regeneration using hyaluronic acid-based hydrogel with bone morphogenic protein-2 and human mesenchymal stem cells, Biomaterials 28 (10) (2007) 1830–1837, https://doi.org/10.1016/j.biomaterials.2006.11.050.
[39] S. Wang, J. Zhao, W. Zhang, D. Ye, X. Zhang, D. Zou, X. Zhang, X. Sun, S. Sun, W. Zhang, C. Yang, X. Jiang, Z. Zhang, Comprehensive evaluation of cryopreserved bone-derived osteoblasts for the repair of segmental mandibular defects in canines, Clin Implant Dent R 17 (4) (2015) 798–810, https://doi.org/10.1111/cid.12164.